Available online at www.sciencedirect.com
ScienceDirect
Ceramics International 36 (2010) 693–698
CERAMICS INTERNATIONAL
www.elsevier.com/locate/ceramint

Synthesis of zinc oxide nanocrystalline powders for cosmetic applications

Chia-Liang Kuo [a], Cheng-Li Wang [b], Horng-Huey Ko [c], Weng-Sing Hwang [a], Kuo-ming Chang [b], Wang-Long Li [d], Hong-Hsin Huang [e], Yen-Hwei Chang [a], Moo-Chin Wang [c,*]

[a] *Department of Materials Science and Engineering, National Cheng Kung University, 1 Ta-Hsueh Road, Tainan 70101, Taiwan*
[b] *Department of Mechanical Engineering, National Kaohsiung University of Applied Sciences, 415 Chien-Kung Road, Kaohsiung 80782, Taiwan*
[c] *Department of Fragrance and Cosmetic Science, Kaohsiung Medical University, 100 Shih-Chuan 1st Road, Kaohsiung 807, Taiwan*
[d] *Institute of Nanotechnology and Microsystems Engineering, National Cheng Kung University, 1 Ta-Hsueh Road, Tainan 70101, Taiwan*
[e] *Department of Electrical Engineering and Department of Chemical and Materials Engineering, Cheng Shiu University, Kaohsiung 83347, Taiwan*

Received 30 June 2009; received in revised form 24 August 2009; accepted 2 October 2009
Available online 4 November 2009

Abstract

The synthesis of zinc oxide (ZnO) nanocrystalline powders for cosmetic applications by a coprecipitation process has been investigated. When the $Zn(OH)_2$ precipitates are calcined at 373 K for 10 min, the crystalline phases comprise the major phase of $Zn(OH)_2$ and the minor phase of ZnO. XRD pattern shows that only ZnO is present and no other phase is detected when the $Zn(OH)_2$ precipitates calcined at 413 K for 10 min. The nanocrystallite size of ZnO increases slightly from 32.3 to 44.3 nm when the calcination temperature increases from 413 to 873 K. The activation energy of ZnO nanocrystallite growth is 2.02 kJ/mol, which reveals that the nanocrystalline ZnO is easily grown at low temperature. The UV transmission of ZnO nanocrystallites in the wavelength range from 290 to 375 nm is about 35%, indicating that the ZnO nanocrystallites have an excellent UV-absorbing capability.

Keywords: Zinc oxide; Cosmetic; Nanocrystallites; Coprecipitation

1. Introduction

Ultraviolet (UV) radiation that reaches the earth and damages skin can be divided into three key wavelengths: (1) UVC (32–280 nm), (2) UVB (280–320 nm), and (3) UVA (320–400 nm). UVA radiation, is a major culprit in photoaging and skin cancers [1]. In addition, UVB, which primarily reaches the top-most layer of skin, is thought to be responsible for acute photodamage, including sunburn and some non-melanoma skin cancers [1]. Hence, protection against both UVA and UVB radiation is very important. Shaath [2] pointed out that sunscreens used for the protection of human skin against the harmful effects of solar radiation must contain certain amounts of UV-absorbing substances. Fine particles of various metal oxides, such as ZnO and TiO_2, are extensively used as agents to attenuate (absorb and/or scatter) the UV radiation, and have many desirable characteristics, such as a long history of topical use, broad spectrum absorption, high photostability and low irritancy [3].

Zinc oxide (ZnO) has a hexagonal wurtzite structure (space group $P6_3mc$) with lattice constants of a and c being 3.250 and 5.207 Å, respectively, a direct band gap of 3.37 eV (368 nm), and large excition binding energy of 60 meV at room temperature [4]. ZnO is used in solar cell windows, piezoelectric transducers, gas sensors, UV light emitting/detecting technology and devices with optoelectronic (UV) properties [5]. Moreover, ZnO is also used as a bright green luminescence phosphor in fluorescent devices [6].

Recently, ZnO nanoparticles have attracted much interest because of their various remarkable chemical and physical properties that are distinctive from those of conventional bulk materials. To date, various methods have been adopted for the preparation of ZnO crystallites including sol–gel method [7], evaporative decomposition of solutions [8], gas-phase reaction [9], wet chemical synthesis [10] and hydrothermal discharging-gas method [11]. However, these methods usually involve high temperatures and sometimes complicated processes, which might result in impurities in the final products [12].

* Corresponding author. Tel.: +886 7 3121101x2366; fax: +886 7 3210683.
E-mail address: mcwang@kmu.edu.tw (M.-C. Wang).

0272-8842/$36.00 © 2009 Published by Elsevier Ltd and Techna Group S.r.l.
doi:10.1016/j.ceramint.2009.10.011

However, in order to obtain ZnO nano-powders with appropriate chemical and optical properties for their intended applications, control of morphology, chemical composition, purity and particle size during synthesis are very important. Several studies have demonstrated that a coprecipitation process has many advantages in obtaining highly crystallized nano-powders with a narrow grain size distribution, high purity and low calcination temperature [13–16]. Specifically, the particle properties of ZnO, such as crystallinity and morphology, can be controlled by adjusting factors such as the source species, pH value, reaction temperature, time, and so on.

In the present study, $Zn(NO_3)_2{\cdot}6H_2O$ and NH_4OH have been used for the synthesis of ZnO nanocrystallites by a coprecipitation process. The main purpose of the present investigation is to examine the effect of various process parameters on the phase transformation and growth of ZnO by thermogravimetric and differential thermal analyses (TG/DTA), X-ray diffraction (XRD), transmission electron microscopy (TEM), electron diffraction (ED), and ultraviolet spectrometry (UVS).

This word will investigate: (i) the thermal behavior of $Zn(OH)_2$, (ii) the phase transformation and growth of nanocrystalline ZnO at various calcination temperatures, and (iii) the UV transmission at 290–400 nm.

2. Experimental procedure

2.1. Sample preparation

The starting materials were reagent-grade $Zn(NO_3)_2{\cdot}6H_2O$ (purity ≧ 98%, supplied by Alfa Aersar, USA) and 25.0 vol% ammonia solution (NH_4OH, supplied by Riedel-de Haën, Germany). 0.05 M and 1.0 vol% aqueous solutions were prepared from reagent-grade $Zn(NO_3)_2{\cdot}6H_2O$ and 25 vol% NH_4OH, respectively. The aqueous solution of 1.0 vol% NH_4OH was then added to $Zn(NO_3)_2{\cdot}6H_2O$ solution slowly at a rate of 0.05 cm^3/min, with vigorous agitation at room temperature. At the end of titration, a syringe was used to minimize the size of falling drops and reduce the local reaction effect. During the whole process, the pH value was kept in a range of 7–10 by adjusting the amount of NH_4OH. The mixed solution was stirred at room temperature for 24 h to obtain white precipitates. After precipitation, the precipitates were washed thoroughly two times with a large amount of ethanol (puirty ≧ 99.85%, supplied by J.T. Baker, USA) to remove NH_4NO_3. Subsequently, the precipitates were freeze dried at 218 K in a vacuum.

2.2. Sample characterization

TG/DTA analyses (SETARAM TGA24 Simultaneous Symmetrical Thermoanalyzer, France) were conducted on a 50 mg precipitate sample at a heating rate of 10 K/min in air with Al_2O_3 powders as a reference material. The calcination temperature was determined from the results of DTA. The crystalline phase was identified using an X-ray diffractometer (XRD, Model Rad IIA, Rigaku Co., Tokyo, Japan) with CuK_α radiation and a Ni filter, operated at 30 kV, 20 mA and a scanning rate of 0.25°/min. The microstructure of the ZnO powders was examined by transmission electron microscopy (TEM), operating at 200 kV. Electron diffraction (ED) was also conducted on the calcined samples. The UV-shielding was measured with a UV transmission spectrometer (Optomerics, SPF-290).

3. Results and discussion

3.1. Thermal behavior of the $Zn(OH)_2$ precipitates

Fig. 1 shows the TG/DTA curves of the precipitates, which were heated from 323 to 1473 K in static air at a heating rate of 10 K/min. The TG curve shows a minor weight loss from 323 to 381 K, followed by a major weight loss up to about 423 K, another weight loss extending up to 518 K, and a small weight loss up to 1273 K. Above 1273 K, there is no further weight loss until 1473 K. The first weight loss (−0.5%) is assigned to the vaporization of absorbed water. The first large weight loss (−8.4%) can be ascribed to the removal of most of the hydroxide radicals in the precipitates. The second large weight loss (−15.6%) between 423 and 518 K is mostly due to the decomposition of amino radicals. Finally, the small weight loss between 518 and 1273 K is due to the removal of residual hydroxide radicals involved in the intermediates.

The DTA result in Fig. 1 also indicates that there are two main endothermic peaks, at 401 and 483 K. The endothermic peak at 401 K is due to the dehydration of the precipitates, while that at 483 K is attributed to the decomposition of NH_2^- into N_2 and H_2 [17].

3.2. Phase evaluation of the $Zn(OH)_2$ precipitates at various calcination temperatures

The XRD patterns of the $Zn(OH)_2$ precipitated at various pH values and calcined at 413 K for 10 min are shown in Fig. 2,

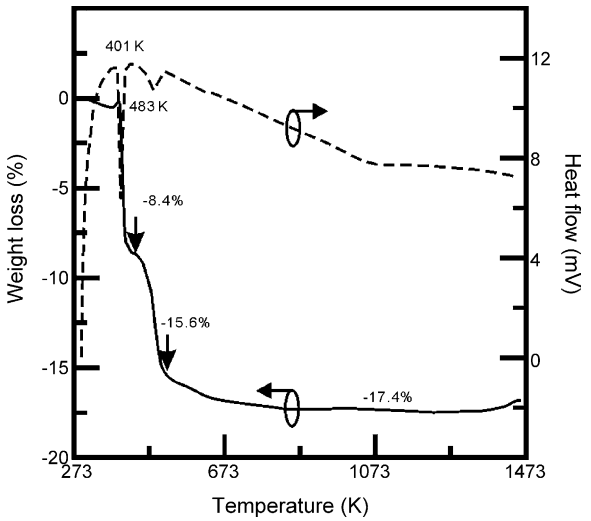

Fig. 1. DTA/TG curves of ZnO precursor powders precipitated at pH 9 with a heating rate of 10 K/min.

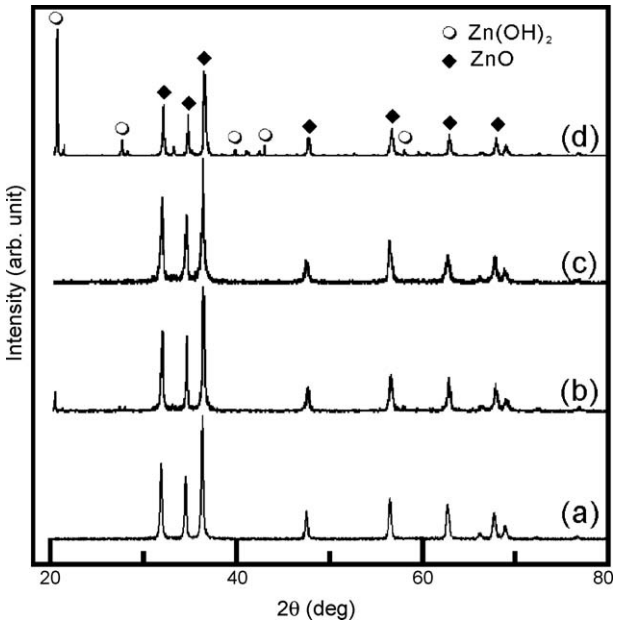

Fig. 2. XRD patterns of ZnO precursor powders precipitated at various pH values and calcined at 413 K for 10 min: (a) pH 7, (b) pH 8, (c) pH 9 and (d) pH 10.

which indicate that all the peaks match well with the wurtzite structure, except those for the precursor precipitated at pH 10 [Fig. 2(d)]. Fig. 2(d) shows that the phases of the calcined powders are ZnO and $Zn(OH)_2$. This is because when the pH is greater than 9, the hydrolysis produces a locally high concentration of bases, favoring the formation of $Zn(OH)_2$.

The results of Fig. 2 indicate that the formation of ZnO or $Zn(OH)_2$ depends on the pH value of solution. Since in pure water, NO_3^- ions hydrolyze and release OH^- ions, then Zn^{2+} ions connect with OH^- and form $Zn(OH)_2$. However, this result is due to the weak hydrolyzing ability of NO_3^- ions, and Zn^{2+} ions are thus the main zinc species in solution [18].

Fig. 3 shows the XRD patterns of the $Zn(OH)_2$ precipitated at pH 7 and calcined at various temperatures for 10 min. Fig. 3(a) indicates that the crystalline phases of the calcined powders comprise the major phase of $Zn(OH)_2$ and the minor phase of ZnO. Moreover, Fig. 3(a) also indicates that the precipitates also contain ZnO as the minor phase. This is because as part of the coprecipitation process, $Zn(OH)_2$ precipitates dissolve in the supersaturated solution, Zn^{2+} complex with OH^- ions, and form $Zn(OH)_4^{2-}$.

$$Zn(OH)_2 + 2H_2O \rightarrow Zn^{2+} + 2OH^- + 2H_2O \rightarrow Zn(OH)_4 + 2H^+ \quad (1)$$

Then, due to the diffusion of ions and deregulation movement among molecules and ions in the solution, clusters of $Zn_xO_y(OH)_z^{(z+2y-2x)-}$ are formed by the dehydration reaction of $Zn(OH)_4^{2-}$. When the particle size of the $Zn_xO_y(OH)_z^{(z+2y-2x)-}$ clusters reaches a certain value, the ZnO nucleus is formed and then the ZnO is precipitated [19].

Fig. 3(b), (C), and (d) shows the XRD patterns of the $Zn(OH)_2$ precipitates calcined at 483, 493 and 503 K for 10 min, respectively. It is found that the crystallinity of the ZnO phase is improved with increasing calcination temperature. When calcined at 513 K for 10 min, only ZnO is present and no other phase is detected, as shown in Fig. 3(e).

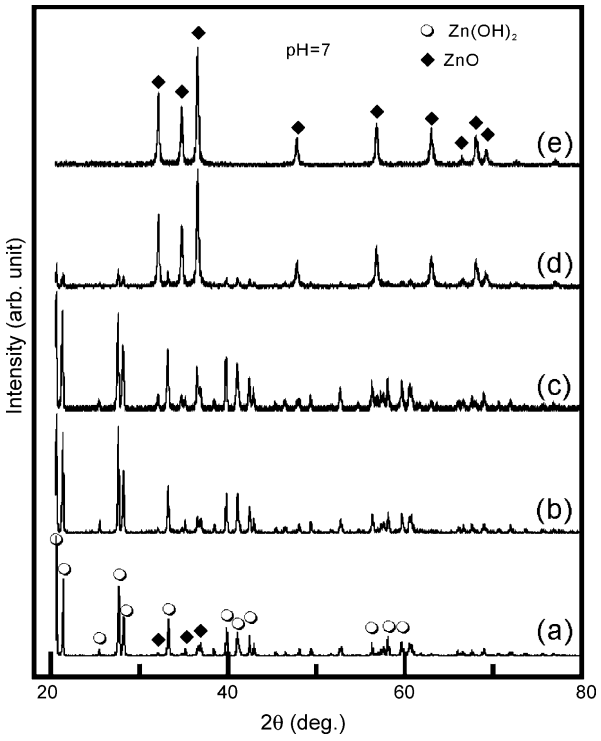

Fig. 3. XRD patterns of the ZnO precursor powders precipitated at pH 7 and calcined at different temperatures for 10 min: (a) 373 K, (b) 383 K, (c) 393 K, (d) 403 K and (e) 413 K.

3.3. Crystal growth of the ZnO nanocrystallite powders

The nanocrystallite sizes of the ZnO powders were obtained when the precipitates post-calcined at various temperatures for 10 min and were calculated by using Scherrer's formula [20]:

$$\alpha = \frac{0.9\lambda}{\beta \cos\theta} \quad (2)$$

where α is the crystallite size of the synthesized ZnO nanoparticles after being calcined at various temperatures for 10 min, $\lambda = 0.15405$ nm is the X-ray wavelength of CuK_α, β is the full width at half maximum intensity, and θ is the Bragg's angle.

The nanocrystallite size depends on calcination temperature for the ZnO precursors precipitated at pH 7 and calcined for 10 min is illustrated in Fig. 4. It is found that the nanocrystallite size of ZnO increases from 32.3 to 44.3 nm when the calcination temperature increases from 413 to 873 K.

The nanocrystallite size (D) and the activation energy (ΔE) for crystal growth can be estimated as [21]:

$$D = A \exp\left[\frac{-\Delta E}{RT}\right] \quad (3)$$

where A is the constant value, R denotes the gas constant and T is the absolute temperature of the crystallite growth.

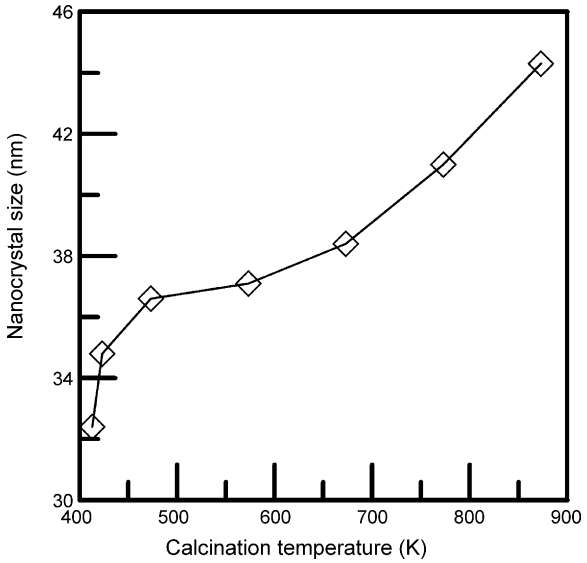

Fig. 4. Nanocrystallite size of ZnO precipitated at pH 7 and calcined at various temperatures for 10 min.

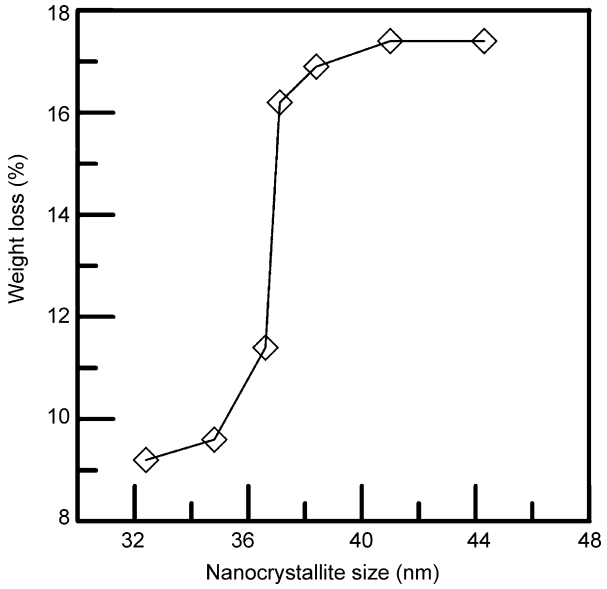

Fig. 6. Size dependence of the relative mass loss for ZnO nanocrystallites at indicated temperatures.

Eq. (4) is obtained from Eq. (3) by taking the logarithm for both sides.

$$\ln D = \frac{-\Delta E}{RT} + \ln A \tag{4}$$

The ln D on the left side of Eq. (4) is plotted against the reciprocal of absolute temperature of crystal growth, and a straight fitting line is obtained, as shown in Fig. 5. The activation energy, namely, 2.02 kJ/mol of ZnO nanocrystallite growth, is obtained from the calculated slope of the straight fitting line. This result reveals that the nanocrystalline ZnO is easily grown at low temperatures.

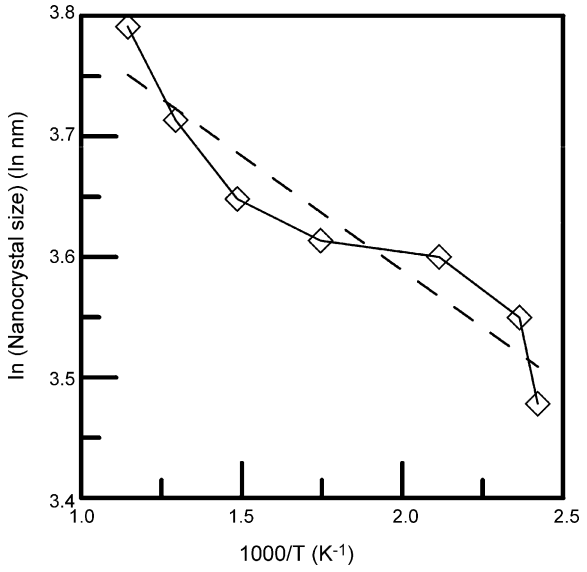

Fig. 5. The ln(nanocrystallite size) and the reciprocal of absolute temperature of crystal growth for ZnO precursor powders precipitated at pH 7 and calcined at different temperatures for 10 min.

According to the results shown in Figs. 1 and 4, it is found that the weight loss depends on the nanocrystallite sizes for ZnO particles at a given temperature: the size dependence of the relative mass for ZnO nanocrystallite at the indicated temperatures is shown in Fig. 6. It can be seen that at high temperatures, all ZnO nanocrystallite undergo large mass losses due to removal of hydroxide radicals. Fig. 6 also indicates that the small crystallite sizes have more hydroxide radicals, while larger particle sizes have less. Therefore, surface hydroxide radicals can be an important component of the ZnO nanoparticles, which likely balance the increased lattice energy at 673 K when ZnO nanocrystallites become smaller [22]. Note that the ZnO nanocrystallites at 673 K did not show any significant changes in sizes. This result is important since the precipitates calcined at 673 K can significantly reduce the hydroxide and amino radicals content while keeping the crystallite size small [22].

3.4. Morphology of the ZnO nanocrystallites after calcination

The TEM bright field (BF) and dark field (DF) images and electron diffraction (ED) pattern of the ZnO precursor powders precipitated at pH 7 and calcined at 413 K for 10 min are presented in Fig. 7. Fig. 7(a) and (b) shows the BF and DF images of the ZnO nanoparticles, indicating that the nanocrystallite size is about 20 nm. Moreover, it is also found that the nanocrystallites are gradually incorporated into large particles. Fig. 7(c) shows the ED pattern of the ZnO nanocrystallites. Fig. 7(d) illustrates the high resolution TEM image of the ZnO nanocrystallite, with the ZnO (2 0 0) spacing of about 0.144 nm indicated by an arrow.

Xu et al. [18] pointed out that aspect ratio of ZnO particles increases by raising the concentration of ammonia solution. In the present study, this low aspect ratio of ZnO nanoparticles

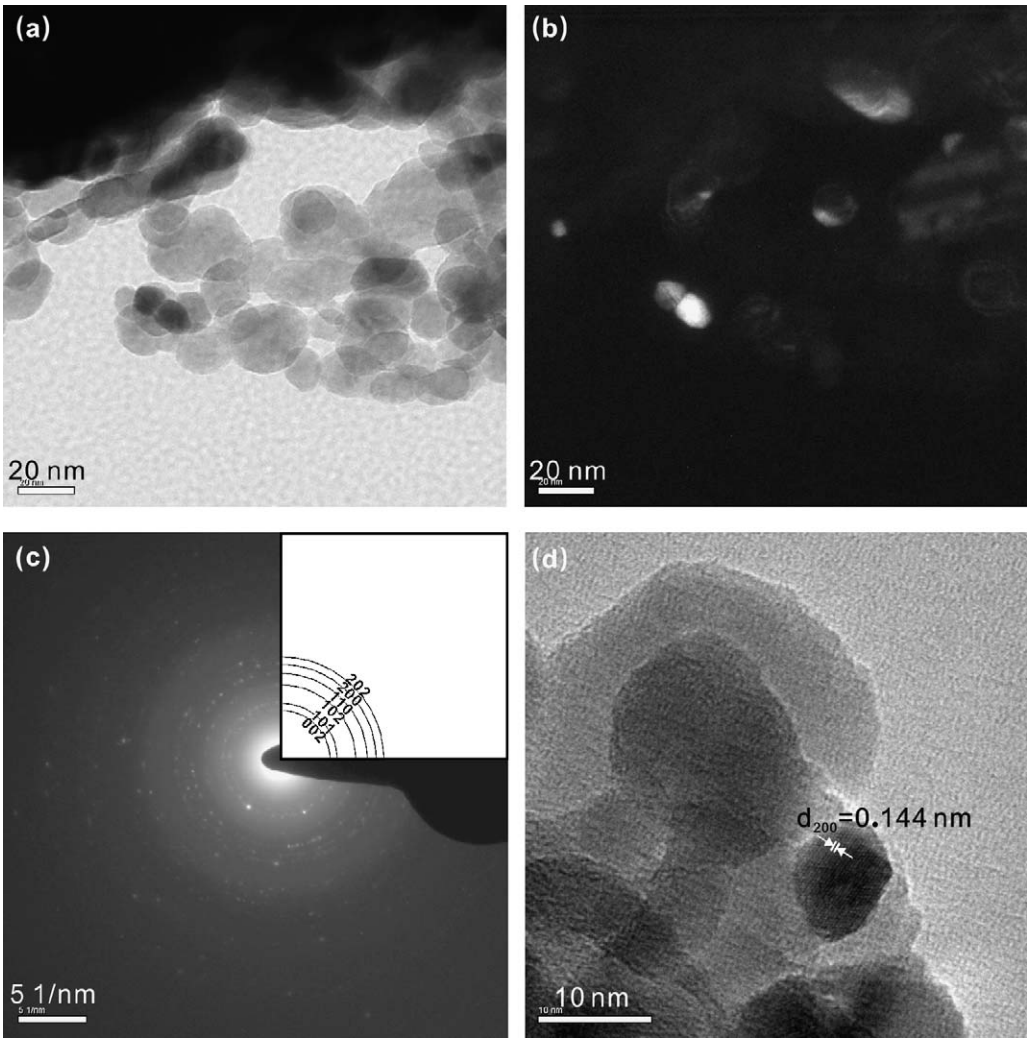

Fig. 7. TEM images and ED patterns of ZnO precursor powders precipitated at pH 7 and calcined at 413 K for 10 min: (a) BF image, (b) DF image, (c) ED pattern of (a), and (d) high resolution image of (a), indicating that of ZnO (2 0 0) spacing.

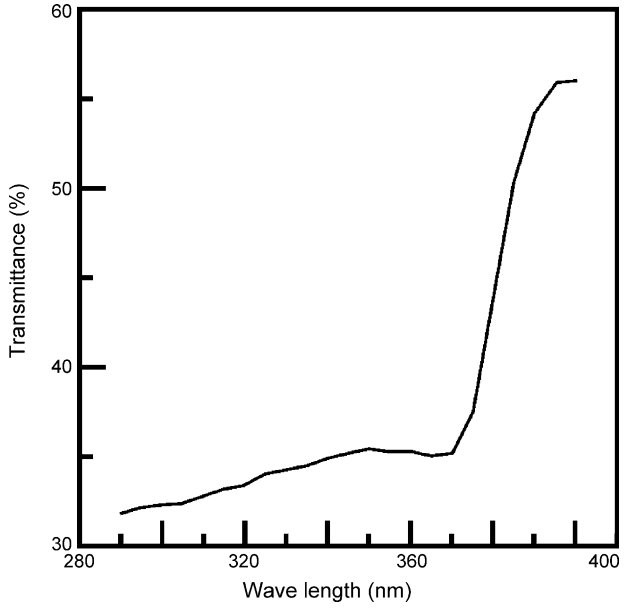

Fig. 8. UV transmittance in the wavelength of 290–400 nm for zinc oxide synthesized at pH 7 and calcined at 413 K for 10 min.

prepared with a medium concentration (pH 7) of ammonia solution is related to its inhibited growth along the *c*-axis.

3.5. The optical properties of ZnO nanocrystallite powders

When the ZnO precursor powders are precipitated at pH 7 and calcined at 413 K for 10 min, the relation between transmissions depends on wavelength in the range of 290–400 nm is shown in Fig. 8. It is found that the transmission of the ZnO nanocrystallite powders in the wavelength range between 290 and 375 nm is below 35%, although, it suddenly increases to 56% as the wavelength rises from 375 to 400 nm.

Fig. 9 shows the relation between average transmission and nanocrystallite size in the wavelength range from 290 to 375 nm for the ZnO precursors precipitated at pH 7 and calcined at various temperatures for 10 min. It reveals that the average transmission increases with the crystallite size. This result indicates that ZnO precursors precipitated at pH 7 and calcined at 413 K for 10 min can be used as a UV-attenuating agent.

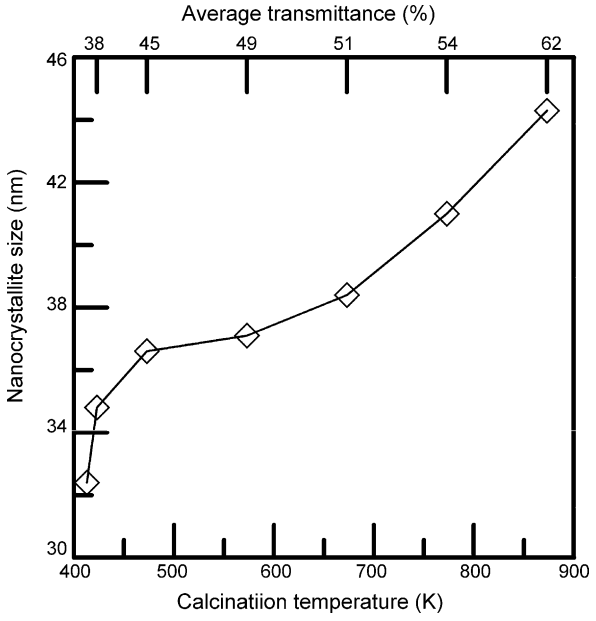

Fig. 9. The nanocrystallite size depends on average transmission in the wavelength range from 290 to 375 nm for ZnO precursor powders precipitated at pH 7 and calcined at various temperatures for 10 min.

4. Conclusions

The ZnO nanocrystalline powders for cosmetic applications have been synthesized at low temperature by a chemical coprecipitation method using $Zn(NO_3)_2{\cdot}6H_2O$ and NH_4OH aqueous solutions as starting materials. The results are summarized as follows:

(1) When the ZnO precursor is precipitated at pH 7–9 and calcined at 413 K for 10 min, the calcined powders only contain ZnO. Moreover, $Zn(OH)_2$ and ZnO are formed for the precursor powders precipitated at pH 10.
(2) The crystalline phases of the calcined powders comprise the major phase of $Zn(OH)_2$ and the minor phase of ZnO when the ZnO precursor powders are precipitated at pH 7 and calcined at 373 K for 10 min. The crystallinity of the ZnO phase is improved with increasing calcination temperature.
(3) The nanocrystallite size of ZnO increases from 32.3 to 44.3 nm as the calcination temperature increases from 413 to 873 K for the precursor precipitated at pH 7.
(4) The transmission of the ZnO nanocrystallite powders in the wavelength range between 290 and 375 nm is below 35%.
(5) The average transmission of the ZnO nanocrystallite powders in the wavelength range between 290 and 375 nm increases with increasing crystallite size.

Acknowledgments

This work was supported by the National Science Council and Kaohsiung Medical University, Taiwan, under Contract Nos. 95-2221-E-037-007 and Q 097038, respectively, which is gratefully acknowledged. The authors sincerely thank Prof. M.P. Hung for advice in the manuscript and preparation and Mr. S.Y. Yau for assistance in TEM.

References

[1] D. Fairhurst, M.A. Mitchnick, in: N.J. Lowe, N.A. Shaath, M.A. Pathak (Eds.), Sunscreen-Development, Evaluation, and Regulatory Aspects, 2nd ed., Marcel Dekker, New York, 1997.
[2] N.A. Shaath, in: N.J. Lowe, N.A. Shaath, M.A. Pathak (Eds.), Sunscreen-Development, Evaluation, and Regulatory Aspects, 2nd ed., Marcel Dekker, New York, 1997.
[3] S.M. Al-Hilli, M. Willamder, Optical properties of zinc oxide nanoparticles embedded in dielectric medium for UV region: numerical simulation, J. Nanoparticle Res. 8 (2006) 79–97.
[4] O. Dulub, L.A. Boatner, U. Diebold, STM study of the geometric and electronic structure of ZnO (0 0 0 1)–Zn, (0 0 0 1)–O, (1 0 1 0), and (1 1 2 0) surface, Surf. Sci. 519 (2002) 201–217.
[5] T. Makino, C.H. Chia, N.T. Tuan, Y. Segawa, M. Kawasaki, A. Ohtomo, K. Tamura, H. Koinuma, Exciton spectra of ZnO epitaxial layers on lattice-matched substrates grown with laser-molecular-beam epitaxy, Appl. Phys. Lett. 76 (2000) 3549–3551.
[6] T. Menmoto, T. Negami, S. Nishiwaki, H. Takakura, Y. Hamakawa, Preparation of $Zn_{1-x}Mg_xO$ films by radio frequency magnetron sputtering, Thin Solid Films 372 (2000) 173–176.
[7] R.J. Lauf, W.D. Bond, Fabrication of high-field zinc oxide varistors by sol–gel processing, Am. Ceram. Soc. Bull. 63 (1984) 278–281.
[8] E. Ivers-Tiffee, K. Seitz, Characterization of varistor-type raw materials prepared by the evaporative decomposition of solutions technique, Am. Ceram. Soc. Bull. 66 (1987) 1348–1388.
[9] S.M. Haile, D.W. Jonhagon, G.H. Wiserm, Aqueous precipitation of spherical zinc oxide powders for varistor applications, J. Am. Ceram. Soc. 72 (1989) 2004–2008.
[10] N.Y. Lee, M.S. Kim, I.-J. Chung, M.-H. Oh, Electrical characteristics and reheat-treatment effects in a ZnO varistor fabricated by two-stage heat-treatment, J. Mater. Sci. 26 (1991) 1126–1130.
[11] W.J. Li, E.W. Shi, Y.Q. Zheng, Z.W. Yin, Hydrothermal preparation of nanometer ZnO powders, J. Mater. Sci. Lett. 20 (2001) 1381–1383.
[12] J. Liu, X. Hung, Y. Li, J. Duan, H. Ai, L. Ren, Large-scale and low-temperatures synthesis of maize-shaped ZnO micron flowers with excellent optical properties, Mater. Sci. Eng. B 127 (2006) 85–90.
[13] M. Castellano, E. Matijevic, Uniform colloidal zinc compounds of various morphologies, Chem. Mater. 1 (1989) 78–82.
[14] T. Tsuchida, S. Kitajima, Preparation of uniform oxide particles by homogeneous precipitation from zinc sulfate and nitrate solutions, Chem. Lett. (1990) 1769–1772.
[15] S.M. Haile, W. Johnson, Aqueous precipitation of spherical zinc oxide powders for varistor application, J. Am. Ceram. Soc. 72 (1989) 2004–2008.
[16] M.E.V. Costa, J.L. Baptista, Characteristics of zinc oxide powder precipitated in the presence of alcohol and amines, J. Eur. Ceram. Soc. 11 (1993) 275–281.
[17] C.L. Kuo, C.L. Wang, T.Y. Chen, G.J. Chen, I.M. Hung, C.J. Shih, K.Z. Fung, Low-temperature synthesis of nanocrystalline lanthanum monoaluminate powders by chemical co-precipitation, J. Alloy Compd. 440 (2007) 367–374.
[18] H.Y. Xu, H. Wang, Y.C. Zhang, W.L. He, M.K. Zhu, B. Wang, H. Yan, Hydrothermal synthesis of zinc oxide powders with controllable morphology, Ceram. Int. 30 (2004) 93–97.
[19] K. Byrappa, M. Yoshimura, Handbook of Hydrothermal Technology: A Technology for Crystal Growth and Materials Processing, William Andrew Publishing, LLC Norwich, New York, 2001.
[20] B.D. Cullity, Elements of X-ray Diffraction, 2nd ed., Addison-Wesley Publishing Company, Reading, MA, 1978, p. 87.
[21] M. Jarcho, C.H. Bolen, M.B. Thomas, J. Bobik, J.F. Key, R.H. Doremus, Hydroxylapatite synthesis and characterization in dense polycrystalline form, J. Mater. Sci. 11 (1976) 2027–2035.
[22] G. Li, L. Li, J. Boerio-Goates, B.F. Woodfield, High purity anatase nanocrystals: near room-temperature synthesis, grain growth kinetics, and surface hydration chemistry, J. Am. Chem. Soc. 127 (2005) 8659–8666.